A Simple Model of the Mass Exchange between the Subtropical and Tropical Ocean

ZHENGYU LIU

UCAR Visiting Scientist Program, Program in Atmospheric and Oceanic Sciences, Princeton University, Princeton, New Jersey

(Manuscript received 18 February 1993, in final form 21 July 1993)

ABSTRACT

A simple ventilated thermocline model is used to study the subtropical–tropical mass exchange. It is found that the water subducted in the western subtropical gyre (recirculating window) tends to recirculate within the subtropical gyre, while the water subducted in the eastern part (exchange window) tends to penetrate equatorward. The exchange window expands with an increased easterly wind or basin width on the southern boundary of the subtropical gyre, but shrinks with an increased wind curl within the subtropical gyre.

Furthermore, the total exchange transport increases with the easterly wind or the width of the basin on the southern boundary of the subtropical gyre, but it is independent of subtropical wind. The ventilation mechanism is important in supporting the exchange transport. For wind with realistic strength at the southern boundary, the reduction of the exchange transport is about 15%–30% of the Ekman transport.

Finally, relative to the exchange transport in the interior of the ocean, the exchange transport through the low-latitude western boundary current decreases with increased total exchange transport.

1. Introduction

The equatorial circulation of the upper ocean and the subtropical thermocline circulation have each been studied extensively [for reviews, see McCreary (1985) and Philander (1990) for the equatorial circulation, and Rhines (1986) and Pedlosky (1991) for the subtropical circulation]. So far, most studies have treated them separately. The linkage between the equatorial and the subtropical circulation has rarely been discussed.

On the other hand, observations have revealed a clear connection between the subtropical and equatorial circulations. Maximum tritium concentrations observed in the equatorial undercurrent (EUC) in the central equatorial Pacific (Fine et al. 1981; Fine 1987) suggest that the water in the North Pacific penetrates into the EUC from the interior of the ocean. Isopycnal analysis of salinity and other tracers (Tsuchiya 1981) shows that the 13°C mode water below the eastern Pacific equatorial thermocline can be traced back to the surface ocean near New Zealand. From the study of ΔC^{14}, Toggeweiler et al. (1989) further pointed out that this connection should be extended farther, to the Circumpolar Current in the south and to the Peru upwelling water near the equator. Hydrographic and direct measurements in the Pacific also show evidence that a substantial portion of water in and below the EUC near the western boundary is supplied from the south by a narrow coastal western boundary current, which can be traced back to the extratropics (Tsuchiya et al. 1989). These observations suggest that the upper equatorial and the subtropical oceans are connected both in the interior and along the western boundary.

Pedlosky (1987) first proposed a mechanism to connect the tropical and extratropical thermocline circulation. In his simple analytical model, subducted extratropical surface waters may eventually reach the equatorial region and join the EUC. This point is supported by recent results from an intermediate two-layer model (McCreary and Yu 1992). We will further investigate the mass exchange between the subtropical and equatorial ocean by means of a simple analytical model as well as GCM experiments. Detailed results from GCM experiments will be reported separately (Liu et al. 1994; Liu and Philander 1994). In this paper, a simple ventilated thermocline model is used to highlight the physical mechanism for the subtropical–tropical mass exchange. The major questions to be addressed are

Which part of the subducted subtropical water penetrates equatorward?

What determines the amount of exchange transport?

What determines the relative contribution to the exchange transport from the interior and western boundary?

This paper is arranged as follows. The model is introduced in section 2. The flow pattern, especially the exchange flow and thermocline structure, is compared with the GCM results in section 3. Section 4 will focus on the physical mechanism determining the mass ex-

Corresponding author address: Zhengyu Liu, Department of Atmospheric and Oceanic Sciences, University of Wisconsin—Madison, Madison, WI 53706-1695.

change and presents the core material of the paper. A summary is given in section 5. A different model is also developed independently by McCreary and Liu (1994). Both models confirm the water exchange between the subtropical and equatorial upper ocean.

2. Model and solution

In the GCM experiments (Liu et al. 1994), it is noticed that outside the equatorial band (beyond 5°), the exchange mass flux occurs mainly through a surface poleward flow and a returning subsurface geostrophic flow. Furthermore, the subsurface geostrophic flow consists of two distinctive layers. The upper layer, which is strongly affected by detrainment process, occupies the upper part of the EUC in the equatorial region. The lower layer, which is mainly adiabatic, extends to the core of the EUC. Hence, it seems proper to simulate the mass exchange process with a 2.5-layer ventilated thermocline model mounted with a surface Ekman layer.

The model is similar to that used by Pedlosky and Robbins (1991). A schematic 3D view of the model geometry is shown in Fig. 1. For simplicity, following Pedlosky and Robbins, the density and depth of the surface layer will be specified. Therefore, the surface layer is active in its dynamics but not its thermodynamics. We should point out one conceptual difference about the surface layer between the present model and the Pedlosky and Robbins model. They concentrated on the enhancement of subduction due to the slope of the bottom of the thermocline and therefore took the surface layer as the late winter mixed layer (well below the surface Ekman layer). Thus, their surface layer is rather deep (more than 100 m), particularly in the northern part of the subtropical gyre. In our model, the surface layer represents the Ekman layer or the layer where the direct wind stress penetrates ($\partial_z \tau \neq 0$). This layer is usually shallow (about 50 m). Due to the inactive thermodynamics, there is no distinction in the physics of the surface layers between the two models.

South of the outcrop line, the momentum equations for each layer are

$$-fv_s\rho_0 = -\partial_x p_s + \partial_z \tau_x, \quad fu_s\rho_0 = -\partial_y p_s + \partial_z \tau_y \quad (2.1)$$

$$-fv_n\rho_0 = -\partial_x p_n, \quad fu_n\rho_0 = -\partial_y p_n, \quad n = 1, 2. \quad (2.2)$$

Here the subscripts s, 1, and 2 represent quantities in the surface layer, layer 1, and layer 2, respectively. Other notations are standard as shown in Fig. 1. In particular, ρ_1 and ρ_2 are constants but ρ_s varies at different locations. For convenience, in most cases, the Coriolis parameter f will be used as the meridional coordinate. The outcrop line and southern boundary of the subtropical gyre (where curlτ = 0) are located at f_o and f_d, respectively.

Since layer 2 represents the lower adiabatic geostrophic layer, we have the potential vorticity conservation

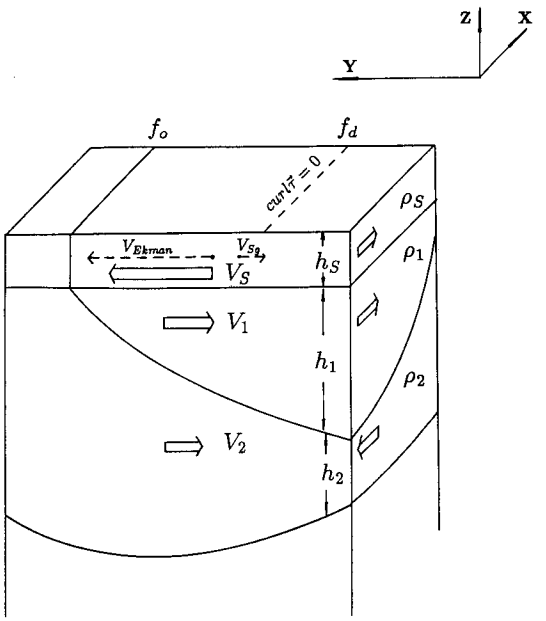

FIG. 1. The 3D geometry of the model, consisting of a surface layer, an upper geostrophic layer (layer 1), and a lower geostrophic layer (layer 2).

$$q_2 = G(p_2), \quad (2.3)$$

with $q_2 = f/h_2$. Here G is an arbitrary function. The zonal domain to be considered is $-60° = x_w < x < 0$. The Sverdrup relation can then be derived as in (A.2).

In the rest of the paper, we consider the case with only a zonal wind stress

$$\tau_x = \tau(y), \quad \tau_y = 0. \quad (2.4)$$

In addition, the density and depth of the surface layer will be specified independent of longitude; that is,

$$\rho_s = \rho_s(f), \quad h_s = h_s(f). \quad (2.5a)$$

To assure gravitational stability, we further assume the surface density structure as

$$\rho_s(f) < \rho_1, \quad f < f_o$$
$$\rho_s(f) = \rho_1, \quad f = f_o$$
$$\rho_1 < \rho_s(f) < \rho_2, \quad f > f_o, \quad (2.5b)$$

where f_o is the outcrop latitude. The thermocline solution is derived in (A.4)–(A.7) for three regions: north of the outcrop line, south of the outcrop line in the ventilated zone, and the shadow zone.

The thermocline solution will be obtained by using the wind stress shown in Fig. 2. The wind has a negative curl from 12°N to the north, representing the subtropical wind. South of 12°N, the easterly wind is "uniform" (no curl), representing the tropical wind. The Ekman pumping is downward everywhere as shown in Fig. 2. The depth and density of the mixed layer in

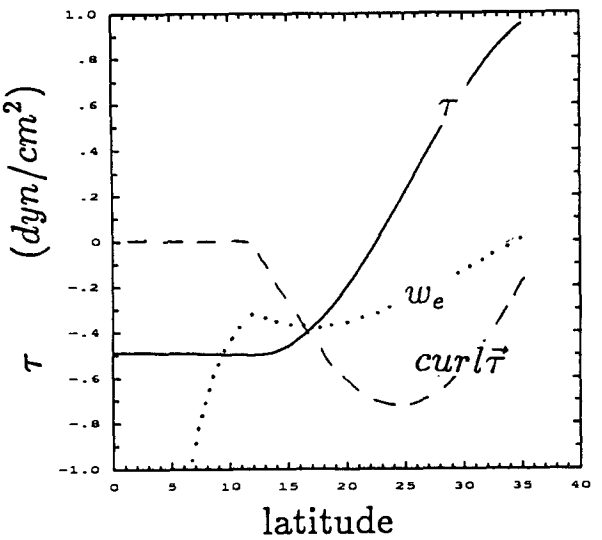

FIG. 2. The wind used in the model study. It shows the zonal wind stress (τ) in dyn cm^{-2}, the Ekman pumping velocity (w_e) in 4×10^{-4} cm s^{-1} and the vorticity of the wind (curl $\vec{\tau}$) in 10^{-8} dyn cm^{-3}. The southern boundary of the subtropical gyre, which is defined by zero wind curl, is at 12°, and the zero wind stress is at about 22°.

(2.5) are given in (A.3). For simplicity, they are chosen such that there is no net zonal transport into the eastern boundary within the surface layer as well as in each geostrophic layer. Thus, the eastern boundary ventilation is absent (Pedlosky 1983; Cessi 1992).

One solution with the outcrop line at 25° is presented in Figs. 3 and 4. Figures 3a and 3b show the layer thicknesses of layer 1 and layer 2. Figures 4a and 4b plot a zonal and a meridional section, respectively. One sees from Fig. 3b that the layer 2 thickness vanishes toward the equator within the ventilation zone; this is the result of potential vorticity conservation (2.3). Along a streamline approaching the equator, the planetary vorticity f decreases. Thus, the conservation of potential vorticity $f/h_2 = \text{const}$ requires that h_2 vanishes on the equator. This singularity is due to the neglect of nonlinearity or mixing processes in the equatorial boundary-layer dynamics (McCreary 1985; Pedlosky 1987), which are absent in the thermocline model (2.1) and (2.2).

3. "Low latitude" thermocline circulation

We first investigate the circulation and structure in the "low latitude" thermocline, which refers to the tropical region outside the equatorial region (beyond 5° up to 12°) in this paper. Particular attention is given to the water exchange flow in this region.

a. Flow field and mass exchange

The streamlines obtained from the solution in Figs. 3 and 4 are presented in Figs. 5a–c for the surface layer at $z = -5$ m, layer 1, and layer 2, respectively. Here, the streamlines in the surface layer are plotted

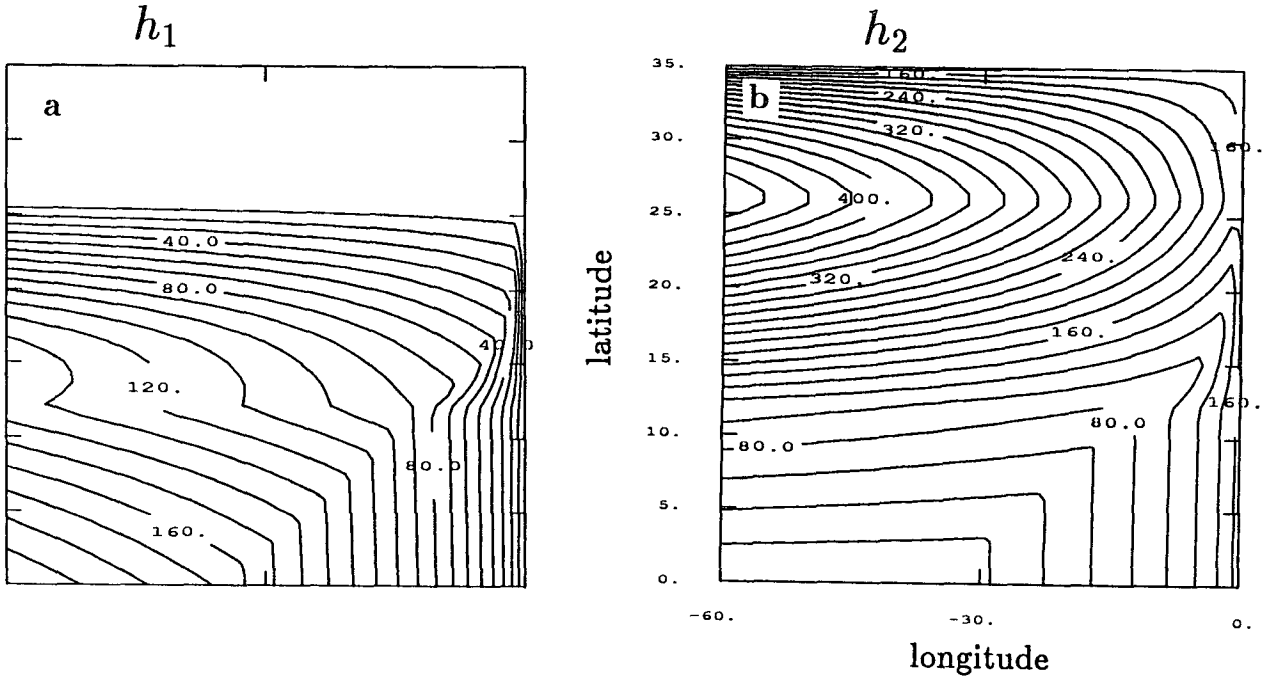

FIG. 3. Layer thickness in meters for the thermocline solution with the outcrop line at $y_o = 25°$, for (a) layer 1 (contour interval 10 m) and (b) layer 2 (contour interval 20 m).

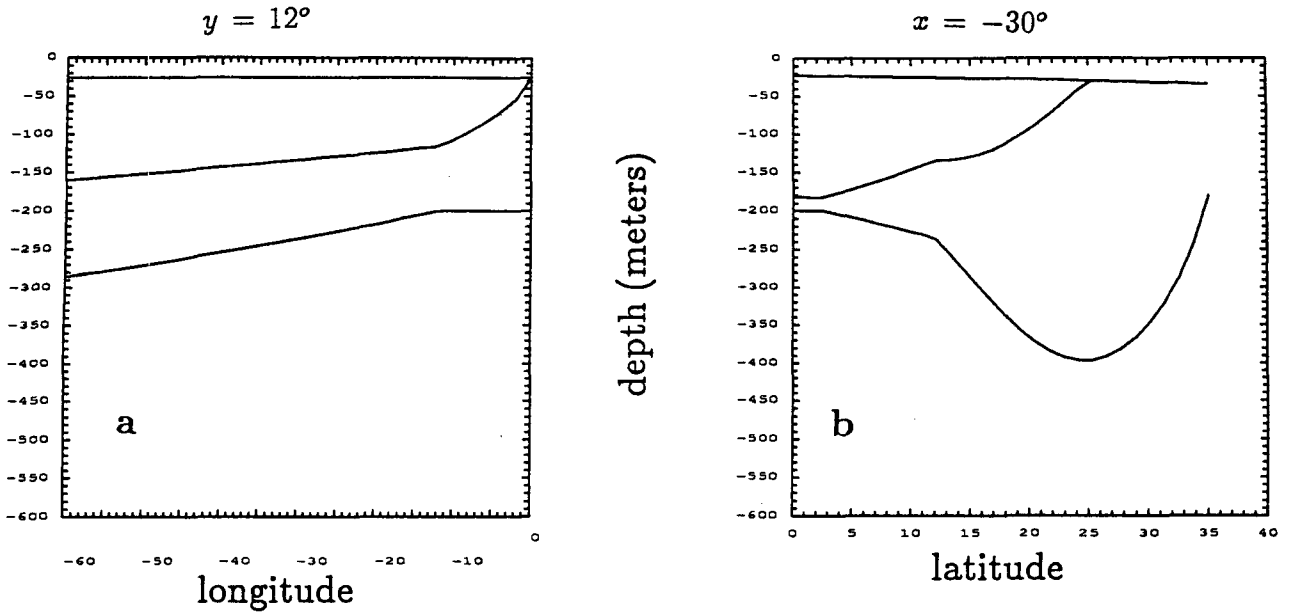

FIG. 4. Layer thickness of the thermocline solution for (a) the zonal section at 12° and (b) the meridional section in the midbasin at 30°.

according to the velocity field, while the streamlines in layer 1 and layer 2 are simply isobars. A GCM experiment was also carried out under the same wind forcing in Fig. 2. [For details of the GCM results, see Liu et al. (1994).] The streamlines are plotted at the depth of $z = -5$ m and on the isotherms of $T = 22.5$°C and $T = 19$°C as in Figs. 5d–f, respectively. The comparison between the theoretical solution in Figs. 5a–c and the GCM results in Figs. 5d–f shows qualitatively good agreement except in the equatorial region.

In particular, the subtropical–tropical exchange flow can be seen clearly in Fig. 5 from both theoretical and GCM solutions. First, the flow from the equator toward the subtropics is shown clearly in Figs. 5a and 5d in the surface. In the interior, the surface water flows northeastward before reaching 12°N and turns abruptly toward northwest, converging at the latitude of zero wind stress (about 22°).

The equatorward flow of subducted subtropical water can be observed in the subsurface layers. In layer 1 and on $T = 22.5$°C surface (Figs. 5b and 5e), the water that subducts in the central and western part of the outcrop line will flow northward after reaching the western boundary. This represents the part of water that will recirculate within the subtropical gyre. In the eastern part, the subducted waters cross the southern boundary of the subtropical gyre and eventually join the EUC. Most of the exchange waters tend to flow equatorward in the interior of the basin. This tendency is related to the exchange flow pattern that changes direction abruptly from southwest to southeast across the southern boundary of the subtropical gyre.[1]

In layer 2 and on $T = 19$°C surface (Figs. 5c and 5f), there is a strong subtropical gyre north of 12°N. Similar to the shallow geostrophic flow (Figs. 5b and 5e), the water subducted in the central western part of the outcrop line will recirculate within the subtropical gyre. In the eastern part, the subducted water penetrates equatorward. However, different from the upper geostrophic flow, this penetrating water tends to flow in the southwest direction. Thus, most of the water flows to the equator through the low latitude western boundary current. The physical mechanisms controlling the water exchange will be discussed in the next section.

Why is there a westward penetrating flow in layer 2, but an eastward penetrating flow in layer 1? This can be explained from our simple model. South of 12°N, there is no barotropic flow due to the vanishing curlτ. In the meridional direction, this is accomplished by a northward flow in the surface layer and southward flows in both subsurface layers. However, in the zonal direction, there is little surface flow because of the absence of meridional wind stress and associated Ekman

[1] The abrupt change of the flow direction is caused by the discontinuity in the curlτ field. Indeed, in the limit of a shallow surface layer, with the aid of (A.1) and (A.8), one can show that $\partial_x h^2 (dx/df)|(p_1 = \text{const}) \sim h^2(-A\tau + \partial_{ff}\tau)$ where $A > 0$ is a function of latitude. Thus, with a vanishing curlτ, $dx/df|_{p_1} \sim 1/\partial_x h < 0$, i.e., layer 1 flows toward the east. Furthermore, one sees that the cusp of the layer 1 streamline in Fig. 5b along 12°N is caused by the discontinuity of $\partial_{ff}\tau$ in the given wind stress (Fig. 2).

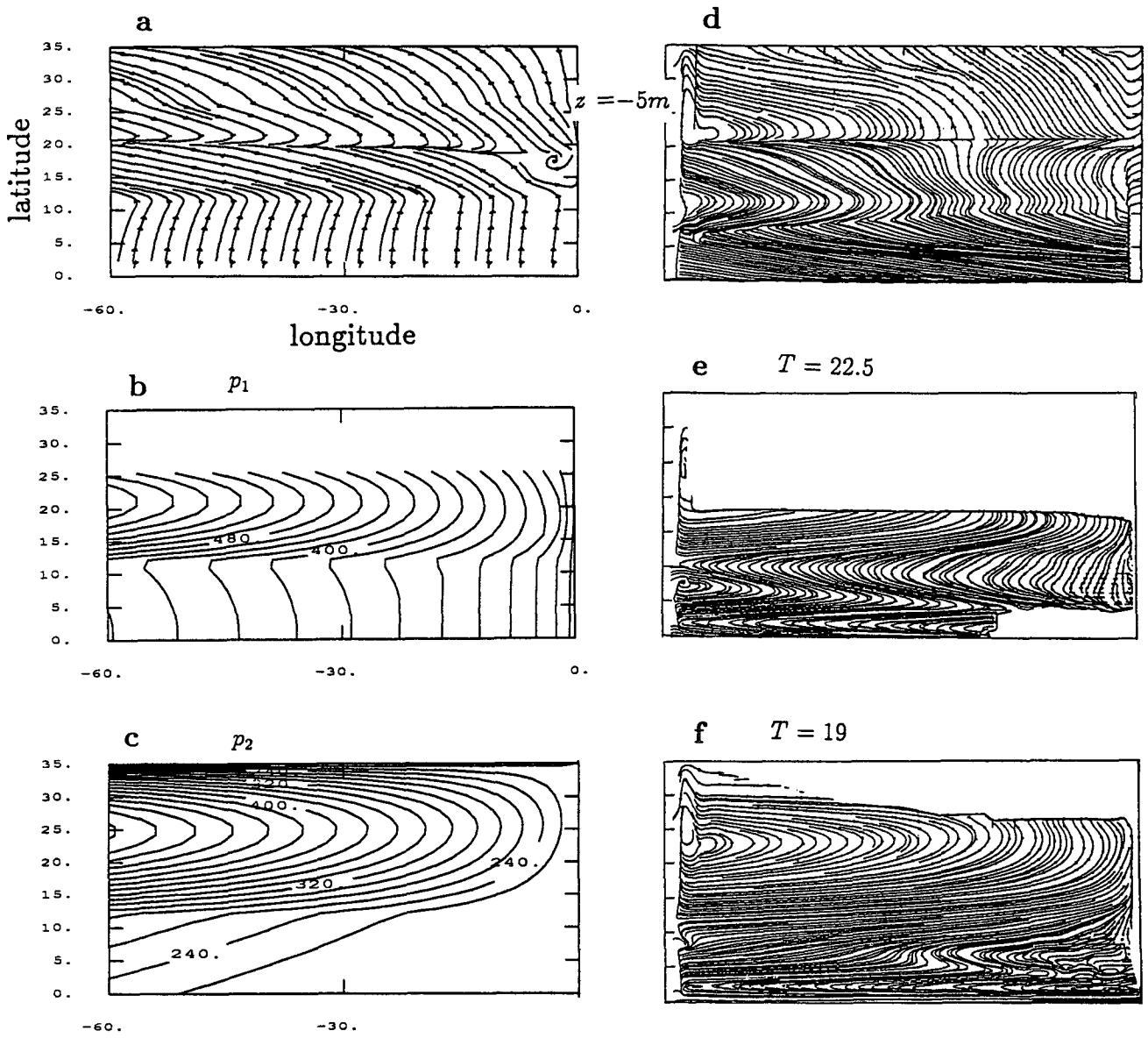

FIG. 5. The streamlines for the simple model solution [(a), (b), and (c)] and for the GCM results [(d), (e), and (f)]. (a) Near surface at $z = -5$ m; (b) layer 1 pressure (dynamic meter); (c) layer 2 pressure; (d) near surface at $z = -5$ m; (e) $T = 22.5$ isotherm; (f) $T = 19$ isotherm. In calculating the velocity in the surface layer of the simple model, we have assumed a linear distribution of the wind stress from surface to the bottom of the surface layer. The streamlines in (a) are plotted according to the total surface velocity vectors at that depth. The streamlines in the GCM run of (d)-(f) are also plotted as contours connecting the horizontal velocity vectors. The surface layers in (a) and (d) show the northward velocity field, while the other panels show the subsurface geostrophic southward return flow.

drift. Thus, the mass flux compensation must occur between the two geostrophic layers. This means that the zonal flow in layer 1 and layer 2 must be in the opposite directions. Furthermore, the downward Ekman pumping associated with the "uniform" easterly wind requires β spiral structure for the vertical variation of horizontal velocity. Thus, the upper layer must be more eastward than the lower layer. In other words, the constraint due to both a zero net zonal flow and the β spiral requires that the upper-layer flow is toward the southeast direction while the lower-layer flow is toward the southwest. The zonal velocity in the surface layer is purely due to the geostrophic component. Since the pressure in the surface layer is close to that in layer 1, the northward surface flow also flows eastward before reaching 12°N (Figs. 5a and 5d).

Finally, the GCM results in Figs. 5e, f show that, in the thermocline, the poleward midlatitude western boundary current is separated from the equatorward low latitude western boundary current at the southern

boundary of the subtropical gyre (where curlτ = 0); this is a robust phenomenon observed in various GCM simulations (e.g., Cox and Bryan 1984; Cox 1985). Yet, there has been no theoretical proof in the case of a baroclinic thermocline flow. Thus, we will take this phenomenon as granted. As far as studying the exchange transport is concerned, this turns out to be one key assumption in our simple model study.

b. *Thermocline structure*

It is also interesting to explain a basic feature associated with the "low latitude" thermocline structure: an equatorward shallowing of the bottom of the lower geostrophic layer, but an equatorward deepening of the upper geostrophic layer. As explained above, layer 2 has to flow westward south of the subtropical gyre. The associated zonal pressure gradient requires that the bottom of layer 2 (at the depth of h) shoals equatorward. However h has to be deeper than the shadow zone thermocline depth on the east (southward geostrophic flow always corresponds to a westward deepening thermocline). In addition, the conservation of potential vorticity in layer 2 requires $h_2 \to 0$ toward the equator. The decreasing of the thickness of layer 2 toward the equator is faster than the shoaling of the total depth. Thus, the depth of layer 1 has to deepen toward the equator.

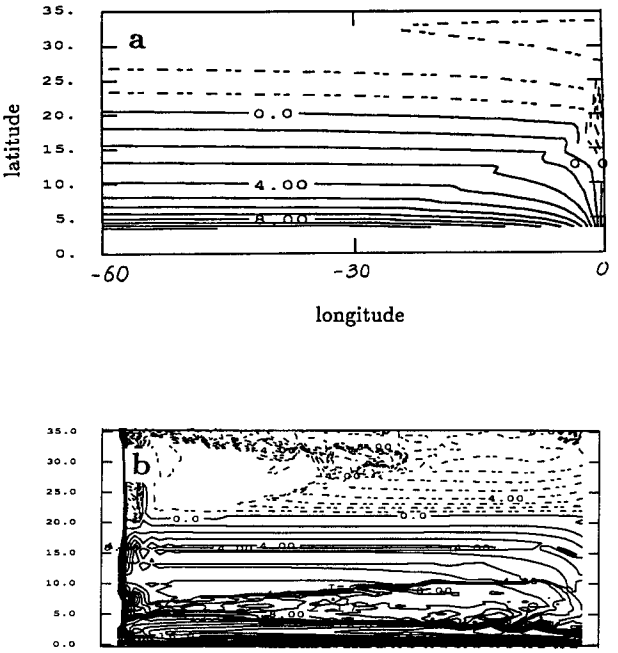

FIG. 6. The surface meridional velocity in cm s^{-1} at $z = -5$ m in the simple model (a) and in the GCM (b). Notice the weaker northward velocity in the eastern part, which is caused by the shadow zone below. In (b), the velocity larger than 20 cm s^{-1} is not drawn.

c. *The surface meridional velocity*

Figure 6a shows the surface meridional velocity component at $z = -5$ m calculated from the theory. The meridional velocity remains unchanged along a latitude circle in the ventilated zone (VZ) (from western boundary eastward). However, within the shadow zone (SZ) (in the southeast) the meridional velocity decreases toward the east. This feature is also evident in the GCM as shown in Fig. 6b. It is therefore curious why the surface meridional velocity is weaker above the shadow zone than above the ventilated zone.

Physically, this can be understood as follows. First, for a thin surface layer, the surface layer pressure is similar to that of layer 1 [see (A.1c)]. The vertically integrated momentum equation of the surface layer and layer 1 is

$$-f\bar{v} = -\partial_x p_1 + \tau/(h_1 + h_s), \qquad (3.1)$$

where $\bar{v} = \int_{-(h_1+h_s)}^{0} v/(h_1 + h_s)$ is the mean velocity in the two layers. In the shadow zone, there is no current in layer 2, so all of the northward flow in the surface layer is returned within layer 1. Thus, $\bar{v} = 0$. Eq. (3.1) degenerates to

$$\partial_x p_1(\mathrm{SZ}) = \tau/(h_1 + h_s). \qquad (3.2a)$$

This states that all of the wind stress is used to build up the zonal pressure gradient at the bottom of layer 1. (Or equivalently, all of the work done by the wind goes to building up available potential energy above the bottom of layer 1.) The result is a strong zonal pressure gradient. In contrast, in the ventilated zone, part of the northward surface flow is compensated in layer 2 through ventilation. Thus, $\bar{v} > 0$. This gives a pressure gradient

$$\partial_x p_1(\mathrm{VZ}) = \tau/(h_1 + h_s) + f\bar{v}. \qquad (3.2b)$$

On a latitude with an easterly wind $\tau < 0$, the comparison of (3.2a) and (3.2b) shows that the pressure gradient is stronger above the shadow zone; that is,

$$|\partial_x p_1(\mathrm{VZ})| < |\partial_x p_1(\mathrm{SZ})|. \qquad (3.2c)$$

Therefore, the southward surface geostrophic flow, which is approximately determined by the pressure gradient in layer 1, is stronger above the shadow zone. This in turn results in a larger reduction of the northward Ekman flow over the shadow zone. Thus, the net surface northward flow is weaker above the shadow zone. This implies that the deep thermocline ventilation enhances the surface branch of the mass exchange transport and therefore the exchange transport itself. We will return to this point later.

4. Subtropical–tropical mass exchange

a. *Ventilation mass exchange*

In the last section (see discussion regarding Fig. 5), we have seen clearly subtropical–tropical mass ex-

change. Based on the fact that the western boundary current separates at the southern boundary of the subtropical gyre, we can further study the physical mechanism for the mass exchange using our simple model.

First of all, at the southern boundary f_d, the surface northward flow will return in both geostrophic layers. It is clear that the necessary condition for layer 2 to exchange water is that the shadow zone boundary $x_S(f)$ [see (A.6)] meets the western boundary south of f_d; that is, $x_S(f_d) \geq x_w$. In the schematic figure of Fig. 7, which plots several possible shadow zone boundaries, case 1 and case 2 satisfy this condition, so mass exchange is possible through the ventilation mechanism. Case 3 does not satisfy this condition. The subsurface exchange mass must be carried diabatically in layer 1 alone.

With (A.6) and (A.2c,d), the condition for ventilation mass exchange can be written as

$$x_S(f_d) = \frac{\rho_o \gamma_1}{2\tau(f_d)} \left\{ \left[\left(1 - \frac{f_d}{f_o}\right) H_0 + \frac{f_d}{f_o} H_s(f_o) \right]^2 - H_s^2(f_d) \right\} \geq x_w. \quad (4.1)$$

In the limit of a vanishing surface-layer thickness ($H_s \to 0$), this gives

$$\left(1 - \frac{f_d}{f_o}\right)^2 H_o^2 \leq \frac{2\tau(f_d) x_w}{\rho_o \gamma_1} \equiv H_C^2. \quad (4.2)$$

This states that, for a fixed wind, basin width and southern boundary f_d, if a layer can exchange mass adiabatically (ventilation) with the tropics, its layer depth has to be shallower than a critical depth $H_c/(1 - f_d/f_o)$. A stronger wind, or a wider basin, or a f_d at a lower latitude, will be able to ventilate a deeper layer to exchange mass with the tropics. A special example is an outcrop line along the southern boundary $f_o = f_d$. Now (4.2) is always satisfied, so the water subducted along the entire f_d will ventilate the tropics.

If (4.2) is satisfied, the lower layer can ventilate into the tropics, eventually reaching the equatorial region. Ventilation can occur either through the low latitude western boundary current or directly through the interior ocean. In our model, the two cases can be distinguished in the following way. If the shadow zone boundary hits the western boundary before reaching the equator, $x_S(0) \geq x_w$ (case 2 in Fig. 7), the ventilation water must flow equatorward through the western boundary. Otherwise, part of the water ventilates the equator through the interior. Replacing f_d by $f = 0$ in (4.2), the criterion for ventilation to the equator through the interior ocean can be written as

$$H_o^2 \leq \frac{2\tau(f_d) x_w}{\rho_o \gamma_1} \equiv H_c^2. \quad (4.3)$$

Therefore, the stronger the easterly wind, or the wider the basin, the more water ventilates the equator through the interior ocean. It should be borne in mind that the criterion (4.3) is much less certain than (4.2), simply because our thermocline model fails near the equator. Nevertheless, it seems that some qualitative features of (4.3) are still valid.

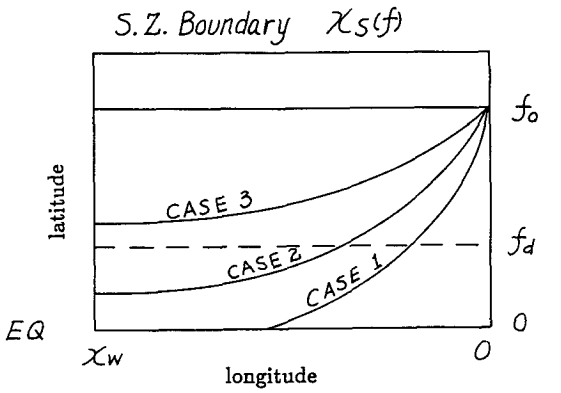

FIG. 7. The schematic figure showing the three cases of shadow zone boundary (of layer 2). Case 1: ventilation to the equator. Case 2: ventilation across the southern boundary of the subtropical gyre, but not to the equator in the interior, so mass exchange occurs through the low latitude western boundary current. Case 3: no ventilation mass exchange.

b. *Mass exchange window*

Figures 5b,c and Fig. 5e, f have shown that the water subducted in the western part of an outcrop line tends to recirculate within the subtropical gyre, while the water subducted in the eastern part tends to penetrate equatorward. The message is that, on the eastern part of an outcrop line, there exists a mass exchange window, within which subducted water will penetrate to the tropics. It is therefore important to know the size of the window and what controls the window size.

To answer these questions, we consider the streamfunction in layer 2 first. There is a critical streamline $x_{d2}(f)$, which meets the western boundary at the southern boundary f_d (see Fig. 8b). Since f_d is assumed to be the separation latitude of the western boundary current in the thermocline, $x_{d2}(f)$ forms the western edge of the mass exchange water in the ventilated zone. Indeed, any streamline flowing to the east of $x_{d2}(f)$ will hit the western boundary south of f_d. By our assumption about the low latitude western boundary current, this streamline will flow toward the equator.

Since layer 2 streamfunction is proportional to h, the critical streamline $x_{d2}(f)$ is determined by

$$h[x_{d2}(f), f] \equiv h(x_w, f_d), \quad (4.4)$$

where h is the solution in the ventilated zone (A.4b). In the case of a shallow surface layer, using the approximate solution in (A.8), (4.4) yields the critical streamline as

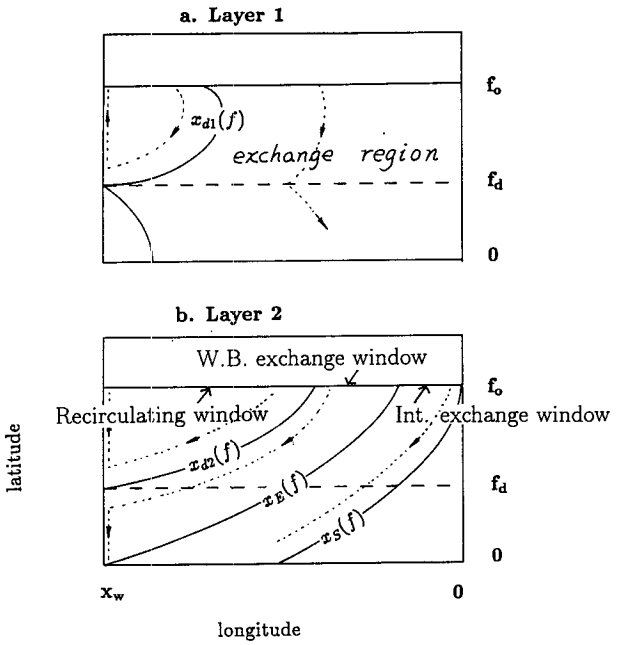

FIG. 8. The schematic figure showing the critical streamlines (solid lines), mass exchange windows (intersection of critical streamlines with the outcrop line) in each layer and streamlines (dashed lines with arrows). (a) Layer 1 critical streamline $x_{d1}(f)$. The mass exchange window is $[x_{d1}(f_o), 0]$. All mass penetrating equator through the interior of the ocean. (b) Layer 2 critical streamlines for mass exchange $x_{d2}(f)$, western boundary mass exchange $x_E(f)$, and the shadow zone boundary $x_S(f)$. The western boundary exchange window is $[x_{d2}(f_o), x_E(f_o)]$, and the interior mass exchange window is $[x_E(f_o), 0]$.

$$x_{d2}(f) = \frac{\gamma_2\rho_0}{2(\tau - f\partial_f\tau)} D_2[x_{d2}(f), f], \quad (4.5a)$$

where

$$\frac{D_2[x_{d2}(f), f] + H_0^2}{1 + (1 - f/f_o)^2\gamma_1/\gamma_2} = \frac{D_2(x_w, f_d) + H_0^2}{1 + (1 - f_d/f_o)^2\gamma_1/\gamma_2}, \quad (4.5b)$$

$$D_2(x_w, f_d) = \frac{2\tau(f_d)x_w}{\gamma_2\rho_0}, \quad (4.5c)$$

where (A.2c,d) and $\text{curl}\tau(f_d) = 0$ have been used. One example of x_{d2} calculated from the simple model is shown as in Fig. 9.

The mass exchange window on the outcrop line is determined by the subduction position of the critical streamline, that is $x_{d2}(f_o)$. This can be obtained from (4.5) after substituting f with f_o as

$$\frac{x_{d2}(f_o)}{x_w} = \frac{\tau(f_d)[1 - (1 - f_d/f_o)^2 H_0^2/H_c^2]}{[\tau(f_o) - f_o\partial_f\tau(f_o)][1 + (1 - f_d/f_o)^2\gamma_1/\gamma_2]}, \quad (4.6a)$$

where H_c is given in (4.2). Noticing (A.2d), we have $\tau(f_o) - f_o\partial_f\tau(f_o) \sim w_e(f_o)$. Hence, on an outcrop line with downward Ekman pumping, it holds that $x_{d2}(f_o)/x_w > 0$. If the ventilation condition (4.2) is satisfied on an outcrop line, the window $x_{d2}(f_o) \leq x \leq 0$ exists on that outcrop line. To the west of the mass exchange window is the recirculating window, from which the subducted water will recirculate within the subtropical gyre (Fig. 8b).

Equation (4.6a) shows one key result of the paper:

$$x_{d2}(f_o) \sim \frac{\tau(f_d)x_w}{w_e(f_o)}. \quad (4.6b)$$

This states that the size of the window is determined by three factors: the local wind at the southern boundary, the width of the basin and the Ekman pumping within the subtropical gyre. The window expands with an increased local wind at f_d or an increased width of the basin, but the window shrinks when the Ekman pumping (or wind curl) within the subtropical gyre increases. The physics can be explained in the following. An increased local wind on the southern boundary or a wider basin increases the Ekman transport across the gyre boundary. This requires more subduction water to return to the tropics. (Here, we have assumed that the exchange mass transport is proportional to the Ekman transport. This will be proven true later.) Thus, the window expands. However, if the Ekman pumping increases within the subtropical gyre, the subtropical gyre is intensified or the velocity in the gyre is increased. Now, if the exchange transport is fixed (the local wind at f_d unchanged), a smaller window is needed to accomplish the transport because of a stronger velocity. This is why the window size is inversely proportional to the subtropical Ekman pumping.

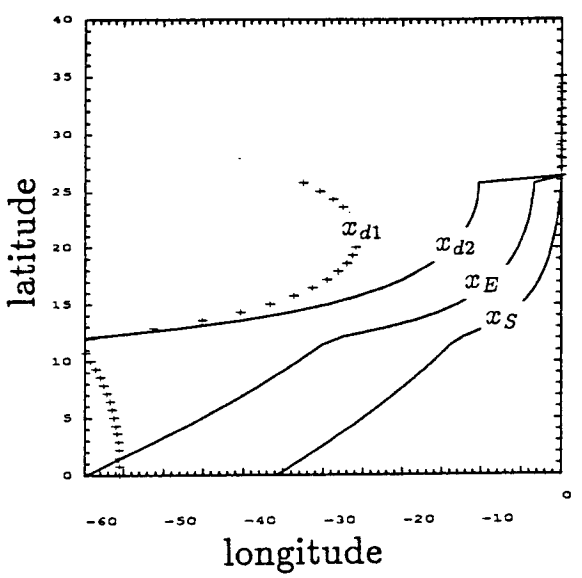

FIG. 9. Critical streamlines for the standard case.

The size of the window also varies with the latitude of the outcrop line according to (4.6a,b). For an outcrop line close to the southern boundary ($f_o \to f_d$), (4.6a,b) shows that

$$\frac{x_{d2}(f_o)}{x_w} \to \frac{x_{d2}(f_d)}{x_w} = 1.$$

This means that the window expands to the whole outcrop line, as expected intuitively. For an outcrop line to the north, the window shrinks toward the eastern boundary because of the increase of the wind curl, which increases $w_e(f_o)$. However, if the outcrop line in the northern part of the subtropical gyre, the wind curl starts to decrease to the north. The window expands again. This is seen clearly in the example in Fig. 10 [the $x_d(f_o)$ line]. Except in the very northern part of the subtropical gyre, this feature agrees excellently with the trajectory analysis in the GCM run of Liu et al. (1993). This latitudinal variation of the window size can also be explained in terms of (4.6). In the midsubtropical gyre, where the local Ekman pumping is strong, the meridional velocity of subduction water is larger. Therefore, only a small window is needed for the mass exchange. To the north and south, the wind curl decreases and so does the meridional velocity of subducted water. Thus, a wider window is needed for the water exchange.

We can also consider the window in the diabatic layer 1. We should first find the critical streamline $x_{d1}(f)$, which meets the western boundary at f_d (see Fig. 8a). One example is shown in Fig. 9 (dotted line). The window on f_o is then given by $x_{d1}(f_o)$. Due to the β spiral structure in the region of downward Ekman pumping, we will always have a wider window on layer 1 than on layer 2; that is,

$$x_{d1}(f_o) < x_{d2}(f_o) < 0. \tag{4.7}$$

c. *The mass exchange through the western boundary and the interior*

The exchange window in layer 2 can be further divided into two subwindows: one exchanges mass through the western boundary, the other through the interior of the ocean. The critical streamline separating the two subwindows is the streamline reaching the western boundary at the equator, denoted by $x_E(f)$. In our model, $x_E(f)$ can be obtained simply by replacing f_d with 0 in (4.5). One example is shown in Fig. 9. The intersection of $x_E(f)$ with the outcrop line is located at $x_E(f_o)$:

$$\frac{x_E(f_o)}{x_w} = \frac{\tau(0)[1 - H_0^2/H_c^2]}{[\tau(f_o) - f_o \partial_f \tau(f_o)][1 + \gamma_1/\gamma_2]}. \tag{4.8}$$

The exchange window $x_{d2}(f_o) \leq x \leq 0$ is then subdivided into the western boundary (WB) exchange window $x_{d2}(f_o) \leq x \leq x_E(f_o)$ and the interior exchange window $x_E(f_o) \leq x \leq 0$.

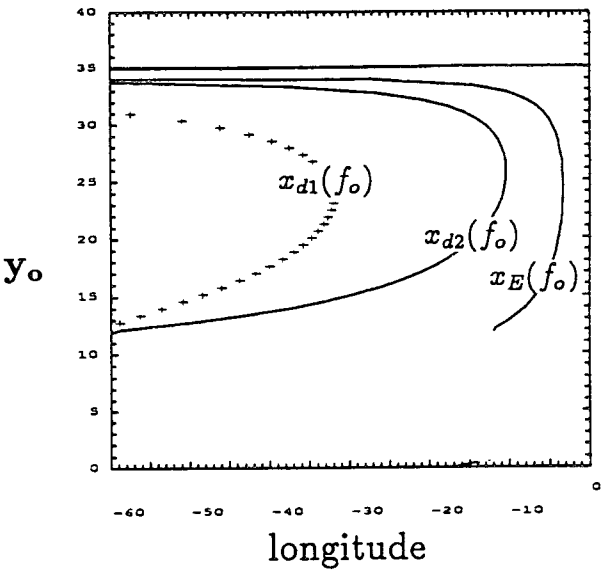

FIG. 10. Under standard wind, the mass exchange window as function of outcrop latitude y_o.

The transport within the western boundary exchange window and interior exchange window can be derived as

$$T_{2\mathrm{WB}} = h^2[x_{d2}(f_o), f_o] - h^2[x_E(f_o), f_o],$$

and

$$T_{2\mathrm{Int}} = h^2[x_E(f_o), f_o] - h^2[0, f_o],$$

respectively, where a common factor is neglected. In the limit of a thin surface layer, with the aid of (4.6a,b), (4.8), (A.2c,d), and (A.8), we have the ratio between the two transports as

$$\frac{T_{2\mathrm{WB}}}{T_{2\mathrm{Int}}} \approx \frac{(H_C/H_0)^2 + 1}{\gamma_2/\gamma_1 (H_C/H_0)^2 - 1}, \tag{4.9}$$

where $H_C = \sqrt{2\tau(f_d)x_w/\rho_o\gamma_1}$ as given in (4.2) or (4.3). In addition, we have used a uniform wind south of f_d [i.e., $\tau(f_d) = \tau(0)$]. Equation (4.9) states that if the wind or the width of the basin [or simply, if the Ekman transport at the southern boundary $\tau(f_d)x_w$] is too small such that the interior ventilation mass exchange condition (4.3) is barely satisfied, $T_{2\mathrm{WB}}/T_{2\mathrm{Int}}$ is very large, implying a dominant western boundary mass exchange in deeper layers. With a stronger wind or a wider basin, H_C increases. The ratio $T_{2\mathrm{WB}}/T_{2\mathrm{Int}}$ decreases, implying an increased interior exchange mass flux relative to the western boundary exchange mass flux. As explained regarding (4.3), this occurs because a stronger wind tends to build a ventilation zone extending farther east near the equator. Thus, more water can joint the EUC from the interior.

Two comments about the subwindows are worth noting. First, in layer 1, there is no western boundary

exchange window. Second, similar to the comment on (4.3), the determination of the subwindow (or x_E) is not reliable due to the failure of the ventilated thermocline near the equator. In comparison, the determination of x_{d2} is more reliable. Therefore, the conclusions derived from (4.9) should be applied cautiously.

d. *Exchange transport*

Now, we discuss the exchange transport. Figure 11 presents the transports of the Ekman drift, the surface layer, layer 1, layer 2, and the total subsurface geostrophic flow (summation of layer 1 and layer 2). The basic features are similar to that of the GCM result (Liu et al. 1994). First, the surface northward transport (in the southern subtropical gyre) is always smaller than the Ekman transport due to the southward geostrophic component in the surface layer as explained in more detail below. Second, the total southward flow, which can be approximated by the total subsurface geostrophic flow, has two peaks in the subtropical gyre and equatorial region, respectively. The exchange transport is represented by the minimum at 12°N. The exchange transport is 8 Sv (Sv $\equiv 10^6$ m^3 s^{-1}), agreeing well with the GCM result.

Finally, we return to the question: what determines the exchange transport at the southern boundary of the subtropical gyre? One usually thinks that the exchange transport is determined by the Ekman transport. However, as seen in Fig. 11 (also true in GCM experiments of Liu and Philander 1994), the northward transport in the surface layer at the southern boundary is always smaller than the Ekman transport. This occurs because the eastward shallowing thermocline produces an opposite southward geostrophic transport in the surface layer. If the wind at the southern boundary increases, the Ekman transport increases. At the same time, however, a sharper thermocline slope is forced, producing a larger southward geostrophic transport in the surface. Therefore, whether or not the total surface-layer northward transport increases depends on the competition between the Ekman drift and the surface geostrophic flow.

We now consider the ratio between the surface geostrophic transport and Ekman (Ek) transport

$$T_{Sg} = \int_{h_s}^{o}\int_{x_w}^{0} v_{Sg}\,dx\,dz, \qquad (4.10a)$$

$$T_{\mathrm{Ek}} = -\tau|x_w|/f. \qquad (4.10b)$$

Figure 12a plots the ratio of transport T_{Sg}/T_{Ek} as a function of the maximum easterly wind stress $\tau_{\mathrm{easterly}} \approx \tau(f_d)$. The maximum westerly τ_{westerly}, which occurs on the northern boundary of the subtropical gyre (see Fig. 2), is fixed in Fig. 12a. To test the sensitivity of our results to different surface-layer depths, three cases are considered with surface-layer depths of 40, 60, and

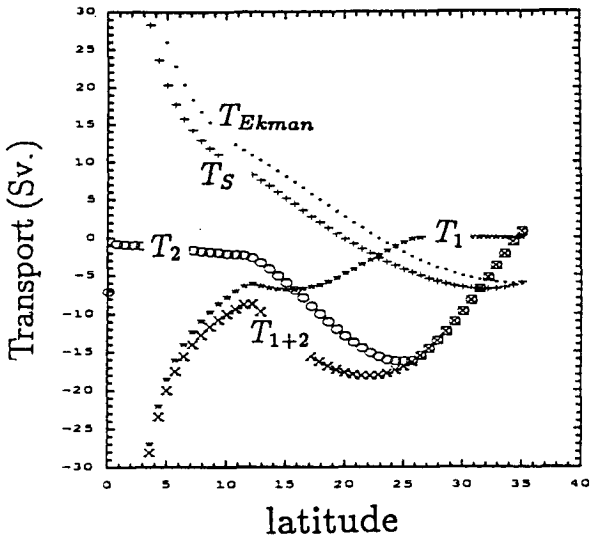

FIG. 11. Various meridional transport (zonally integrated) as function of latitude, where T_{Ek}, T_S, T_1, T_2, and T_{1+2} are the transport of Ekman drift, surface layer, layer 1, layer 2, and the sum of layer 1 and layer 2, respectively. The unit is Sv.

80 m.[2] The most salient feature in Fig. 12a is that the T_{Sg}/T_{Ek} decreases with the strength of the easterly wind. This can be explained by the following. The Ekman transport in (4.10b) is linearly proportional to the wind stress. The surface geostrophic velocity, however, is roughly proportional to the square root of the wind stress because the pressure or the layer depth is usually the square root of wind strength [see (A.4), (A.5) and (A.7)]. (A handwaving argument for $T_{Sg} \sim v_S \sim \delta h \sim \sqrt{\tau x_w}$ is that the work done by the wind is balanced by the available potential energy in the thermocline; i.e., $\delta h^2 \sim \tau x_w$.) Therefore, as the easterly wind increases, the Ekman transport increases faster than the geostrophic transport.

In contrast, if the wind within the subtropical gyre changes, the exchange transport on the southern boundary remains almost unchanged. This is clearly seen in Fig. 12b, which is similar to Fig. 12a but now subject to the change of the westerly wind stress (and therefore the subtropical wind), with the easterly wind fixed.

The other interesting feature in Fig. 12a is the abrupt decrease of the transport ratio at about $\tau_{\min} = -0.2$ dyn cm^{-2}. This implies that for easterly wind weaker than $= -0.2$ dyn cm^{-2}, the Ekman transport will be reduced dramatically. In contrast, for winds stronger than -0.2 dyn cm^{-2}, the reduction of the Ekman transport does not vary much with different easterlies,

[2] The Ekman transport is independent of the depth of the surface layer, while the surface geostrophic transport increases with the layer thickness. Thus, the transport ratio T_{Sg}/T_{Ek} increases with the depth of the surface layer.

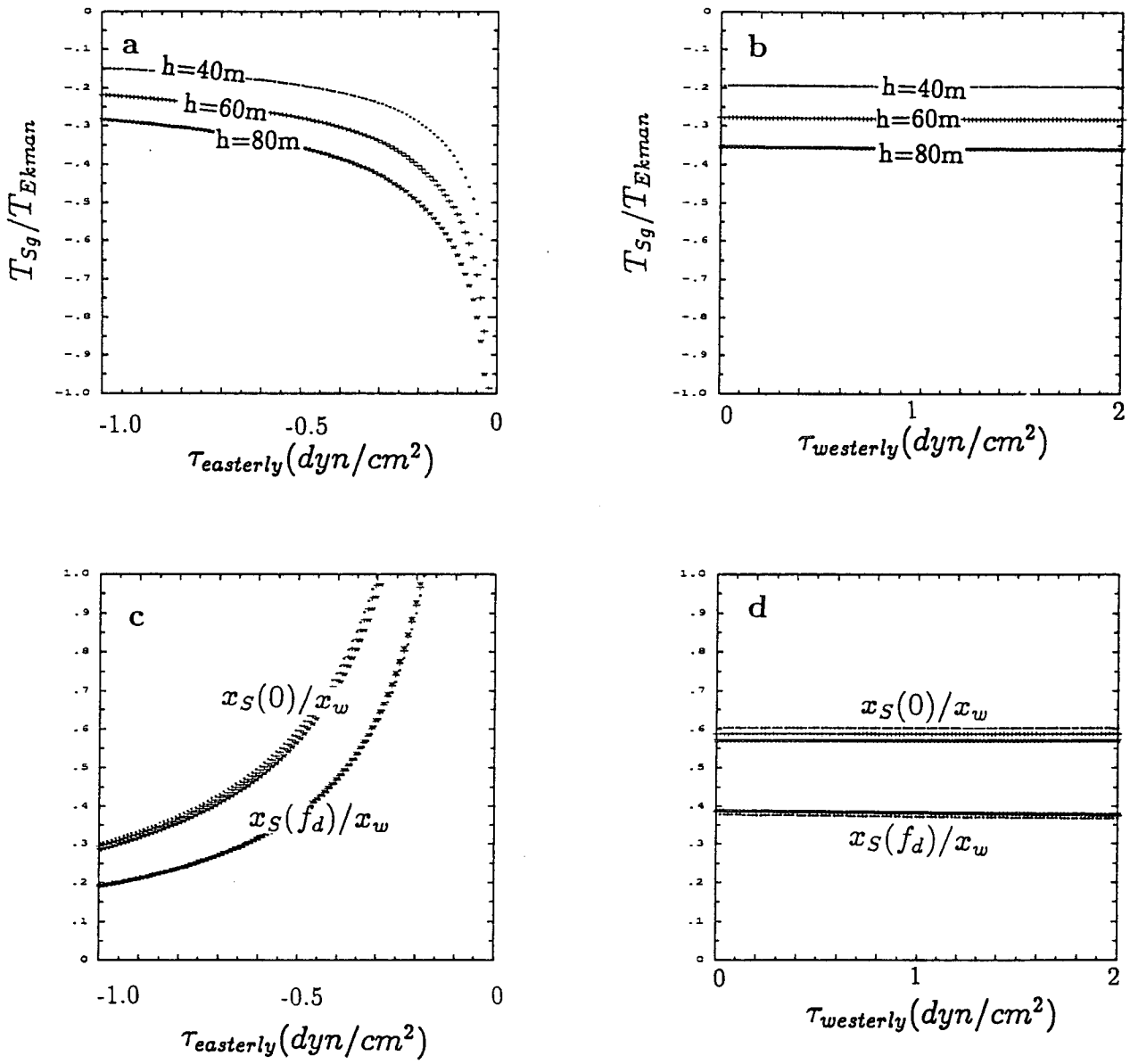

FIG. 12. (a) and (b) The transport ratio between the surface geostrophic transport T_{Sg} and the Ekman transport T_{Ek} for three surface-layer depths: h = 40, 60, and 80 m. In (a) the transport ratio is plotted against the maximum easterly wind stress for wind pattern in Fig. 2 while the maximum westerly wind in the subtropical gyre is fixed; in (b) the transport ratio is plotted against the maximum westerly wind in the subtropical gyre while the maximum easterly wind in the tropics remains unchanged. (c) and (d) The plot of the shadow zone boundary at the equator $x_S(0)/x_w$ and at the southern boundary of the subtropical gyre $x_S(f_d)/x_w$ against the maximum easterly in (c) and against the maximum westerly in (d) for the three choices of mixed layer depths as in (a) and (b).

ranging from about 15% to 30% in the case illustrated. The example shown in Fig. 11 belongs to the stronger wind case.

To explain the dramatic reduction of Ekman transport, let's first study Fig. 12c, which shows the position of the shadow zone boundary at the southern boundary f_d (and on the equator) with respect to different easterly wind strength. At about $\tau_{\text{easterly}} = -0.2$ dyn cm^{-2}, the shadow zone boundary meets the western boundary on f_d. The ventilation mass exchange condition (4.2) is no longer satisfied. There is no ventilated zone south of f_d. In other words, there is no ventilation mass exchange. As has been discussed regarding Fig. 6, the absence of ventilation in layer 2 will reduce the surface velocity, and therefore the surface northward transport significantly. Thus, the dramatic reduction for weak winds occurs because of the lack of ventilation mass exchange in layer 2. In contrast, when the westerly wind

(or the wind within the subtropical gyre) varies, the shadow zone boundary is hardly changed as shown in Fig. 12d. This is consistent with the nearly constant transport ratio shown in Fig. 12b.

In short, ventilation enhances the mass exchange significantly. The critical wind strength for ventilation mass exchange also depends on the width of the basin. Indeed, it is the work done by the wind across the basin τx_w that determines the pressure and therefore the geostrophic velocity [see (A.4), (A.5), and (A.7)]. Thus, in a wider basin, the critical easterly wind is smaller, and vice versa. The implication is that in the Pacific, the exchange transport is stronger than in the Atlantic and the Indian Ocean.

5. Summary

A ventilated thermocline model is used to study the subtropical–tropical mass exchange. The simple model reproduces many basic features of the GCM results except near the equator. In addition, the simple model shed light on the physics of the mass exchange process. The major conclusions are the following.

A typical outcrop line in the subtropical gyre usually has two windows. The western part is the recirculating window, in which subducted waters will recirculate within the subtropical gyre. To the east is the mass exchange window, in which subduction waters will penetrate equatorward. This window can be future divided into two subwindows. The eastern one is the western boundary exchange window, from which waters join the EUC through the low latitude western boundary current; the western one is the interior exchange window, from which waters join the EUC through the interior of the ocean.

The mass exchange window on an outcrop line expands toward the west with an increased easterly wind, or a wider basin on the southern boundary of the subtropical gyre. But, the window shrinks toward the eastern boundary with an increased Ekman pumping within the subtropical gyre.

The exchange transport increases with the easterly wind on the southern boundary of the subtropical gyre, but is independent of the subtropical wind. The ventilation in the deeper thermocline is important in supporting the mass exchange. For winds with realistic strength, the reduction of the exchange transport is about 15%–30% of the Ekman transport.

In the deeper thermocline layers, the interior exchange transport increases relative to the western boundary mass exchange transport with an increased wind or a wider basin. This result suggests that the Pacific should have more mass exchange in the interior of the ocean than the Atlantic or the Indian Ocean.

The insensitivity of the exchange transport to the subtropical wind has an important implication for the strength of the EUC. As analyzed in Liu et al. (1994), the western part of the EUC is dominated by the exchange water with a subtropical source. If the exchange transport does not vary with the wind in the subtropical gyre, the transport of the EUC seems unlikely to change either. In another paper (Liu and Philander 1994), this is indeed shown to be true for a set of GCM experiments.

Acknowledgments. The author is indebted to Drs. G. Philander and J. Pedlosky for many helpful discussions. The author also thanks Dr. S. Carson for suggestions and careful reading. The comments from two anonymous reviewers are also appreciated. During the course of the work, the author was supported by a NOAA postdoctoral fellowship on climate change. The publication of this paper is supported by UCAR.

APPENDIX

The Thermocline Solution

For completeness, we briefly describe the thermocline solution here. The approach is similar to Pedlosky and Robbins (1991). Assuming a motionless abyss below layer 2, one obtains the dynamic pressure in each layer as

$$\frac{p_2(x, y)}{\rho_o} = \gamma_2 h \tag{A.1a}$$

$$\frac{p_1(x, y)}{\rho_o} = \gamma_2 h + \gamma_1(h_1 + h_s) \tag{A.1b}$$

$$\frac{p_s(x, y, z)}{\rho_o} = \gamma_2 h + \gamma_1(h_1 + h_s) + \gamma_{1s}(h_s + z), \tag{A.1c}$$

where

$$\gamma_n = g(\rho_{n+1} - \rho_n)/\rho_o, \quad n = 1, 2$$

$$\gamma_{ns} = g(\rho_n - \rho_s)/\rho_o$$

$$h = h_s + h_1 + h_2.$$

By virtue of (2.1), (2.2), and (A.1), the Sverdrup relation can be derived as

$$h^2 + \frac{\gamma_1}{\gamma_2}(h_1 + h_s)^2 = D_2(x, f) + H^2 + \frac{\gamma_1}{\gamma_2}(H_1 + H_s)^2, \tag{A.2a}$$

where

$$H_* = h_*|_{x=0}, \quad * = s, 1, 2 \tag{A.2b}$$

$$D_n(x, f) = = \frac{2f^2}{\beta\gamma_n} w_e(f)x \tag{A.2c}$$

$$w_e(f) = \text{curl}\left(\frac{\vec{\tau}}{\rho_o f}\right) \equiv \frac{\beta}{f^2\rho_o}(\tau - f\partial_f\tau). \tag{A.2d}$$

In deriving (A.2a), we have used a surface layer with density and depth independent of longitude [see (2.5)]; in (A.2c,d), we have used a zonal wind independent of longitude [see (2.4)].

The eastern boundary condition is simply chosen as no net zonal flow within the surface layer; that is,

$$\int_{-h_s}^{0} u_s dz = 0.$$

With the aid of (2.1b), this can be satisfied with the layer thickness at the eastern boundary of

$$H = H_0 = \text{const} \tag{A.3a}$$

$$H_1 = 0, \tag{A.3b}$$

and

$$H_s(f) = \begin{cases} H_{s0}/\sqrt{1 + \gamma_s(f)/\gamma_2}, & f < f_o \\ H_{s0}\sqrt{\gamma_s(f)/\gamma_1}, & f \geqslant f_o, \end{cases} \tag{A.3c}$$

where H_{s0} = const is the surface-layer thickness at the outcrop line f_o, and $\gamma_s(f)$ is chosen as a linear function. Remember the depth of the surface layer is independent of longitude, so we have $h_s(f) = H_s(f)$. The surface layer depth deepens slowly toward the north along the eastern boundary because the density increases toward the north. A steeper H_s than that in (A.3c) implies upwelling from lower layers and vice versa.

Using potential vorticity conservation of layer 2 in (2.3), we have the solution in the ventilated zone as

$$h_1 + h_s = \left(1 - \frac{f}{f_o}\right)h + \frac{f}{f_o} h_s(f_o) \tag{A.4a}$$

$$h^2 + \frac{\gamma_1}{\gamma_2}\left[\left(1 - \frac{f}{f_o}\right)h + \frac{f}{f_o} h_s(f_o)\right]^2 = D_2 + H^2 + \frac{\gamma_1}{\gamma_2} H_s^2. \tag{A.4b}$$

The quadratic equation for h in (A.4b) can be solved easily.

In the shadow zone, we have the solution

$$h = H = H_0 \tag{A.5a}$$

$$(h_1 + h_s)^2 = D_1(x, f) + H_s^2, \tag{A.5b}$$

where D_1 is defined in (A.2d). The shadow zone boundary is determined by

$$D_1[x_s(f), f] = \left[\left(1 - \frac{f}{f_o}\right)H_0 + \frac{f}{f_o} H_s(f_o)\right]^2 - H_s^2(f). \tag{A.6}$$

North of the outcrop line, layer 1 disappears. The solution is

$$h^2 = D_2 + H_0^2 \tag{A.7a}$$

$$h = h_2 + h_s. \tag{A.7b}$$

In the examples, the parameters are chosen as: $\gamma_2 = \gamma_1 = 1$ cm s^{-2}, $\gamma(f) = \gamma_1(f_o - f)(f_n)$, $H_1 = 0$, $H_2 = 300$ m. Here f_n is the Coriolis parameter at 40°N.

Many important features in the text can be explained in the limiting case of a shallow surface layer, $H_{s0}/H_0 \to 0$. Now, the solution becomes a classical 2.5-layer ventilated thermocline model (Luyten et al. 1983). The solution in the ventilated zone in (A.4b) is simplified as

$$h^2(x, f) = \frac{D_2(x, f) + H_0^2}{1 + (1 - f/f_o)^2 \gamma_1/\gamma_2}. \tag{A.8}$$

In other regions, solutions can be obtained easily by setting $H_s = 0$ in (A.4a), (A.5), (A.6), and (A.7).

In the examples, the parameters are chosen as: $\gamma_2 = \gamma_1 = 1$ cm s^{-2}, $\gamma(f) = \gamma_1(f_o - f)(f_n)$, $H_1 = 0$, $H_2 = 300$ m. Here f_n is the Coriolis parameter at 40°N.

REFERENCES

Cessi, P., 1992: Ventilation of eastern subtropical gyres. *J. Phys. Oceanogr.*, **22,** 683–685.

Cox, M. D., 1985: An eddy resolving numerical model of the ventilated thermocline. *J. Phys. Oceanogr.*, **15,** 1412–1324.

——, and K. Bryan, 1984: A numerical model of the ventilated thermocline. *J. Phys. Oceanogr.*, **14,** 674–687.

Fine, R. A., 1987: The penetration of tritium into the tropical Pacific. *J. Phys. Oceanogr.*, **17,** 553–564.

——, J. L. Reid, and H. G. Ostlund, 1981: Circulation of tritium in the Pacific Ocean. *J. Phys. Oceanogr.*, **11,** 3–14.

Liu, Z., and S. G. H. Philander, 1994: How different wind stress patterns affect the tropical–subtropical circulations of the upper ocean. *J. Phys. Oceanogr.*, **24,** in press.

——, G. S. H. Philander, and R. C. Pacanowski, 1994: A GCM study of subtropical–tropical upper ocean mass exchange. *J. Phys. Oceanogr.*, **24,** submitted.

Luyten, J., J. Pedlosky, and H. Stommel, 1983: Ventilated thermocline. *J. Phys. Oceanogr.*, **13,** 292–309.

McCreary, J., 1985: Modeling equatorial ocean circulation. *Annu. Rev. Fluid Mech.*, **17,** 359–409.

——, and Z. Yu, 1992: Equatorial dynamics in the 2.5 layer model. *Progress in Oceanography,* Pergamon Press.

——, and P. Lu, 1994: On the interaction between the subtropical and equatorial ocean circulations: The subtropical cell. *J. Phys. Oceanogr.*, **24,** 466–497.

Pedlosky, J., 1983: Eastern boundary ventilation and the structure of ventilated thermocline. *J. Phys. Oceanogr.*, **13,** 2038–2044.

——, 1987: An inertial theory of the equatorial undercurrent. *J. Phys. Oceanogr.*, **17,** 1978–1985.

——, 1991: The dynamics of subtropical ocean circulation. *Science,* **248,** 316–322.

——, and P. Robbins, 1991: The role of finite mixed layer thickness in the structure of the ventilated thermocline. *J. Phys. Oceanogr.*, **21,** 1018–1031.

Philander, S. G. H., 1990: *El Niño, La Niña and the Southern Oscillation.* Academic Press, 293 pp.

Rhines, P. B., 1986: The vorticity dynamics of ocean circulation. *Annu. Rev. Fluid Mech.*, **18,** 433–447.

Toggeweiler, R., K. Dixon, and W. S. Broecker, 1989: The Peru upwelling and the ventilation of the South Pacific Thermocline. *J. Geophys. Res.*, **96,** 20 467–20 497.

Tsuchiya, M., 1981: The origin of the Pacific 13°C water. *J. Phys. Oceanogr.*, **11,** 794–812.

——, M., R. Lukas, R. A. Fine, E. Firing, and E. Lindstrom, 1989: Source waters of the Pacific equatorial undercurrent. *Progress in Oceanography,* Vol. 23, Pergamon, 101–147.